Trapping an Elusive Fe(IV)-Superoxo Intermediate Inside a Self-Assembled Nanocage at Room Temperature

Rahul Gera,[†¶] Kundan K. Singh,[‡] Sayam Sen Gupta,[‡§] and Jyotishman Dasgupta[†*]

[†]Department of Chemical Sciences, Tata Institute of Fundamental Research, Mumbai 400005, India.

[‡]Chemical Engineering Division, CSIR-National Chemical Laboratory, Pune, Maharashtra 411008, India

[§]Department of Chemical Sciences, Indian Institute of Science Education and Research Kolkata, Mohanpur, West Bengal, India-741246

Supporting Information Placeholder

ABSTRACT: Natural metalloenzymes stabilize reactive intermediates through specific metal-substrate interactions in protein confinement. Using the structural blueprint of enzyme pockets it is possible to trap elusive intermediates inside molecular cavities. Here we demonstrate room temperature trapping of a rare yet stable Fe(IV)-superoxo ([$Fe^{IV}(O_2)$-bTAML] or **1-O_2**) intermediate subsequent to dioxygen binding at the Fe(III) site of a $(Et_4N)_2$[Fe^{III}(Cl)(bTAML)] (**1-Cl** $[Et_4N]_2$**)** catalyst confined inside the hydrophobic interior of a water-soluble $Pd_6L_4^{12+}$ nanocage.

Iron-based oxygenase family of enzymes activates dioxygen (O_2) gas to carry out chemoselective catalytic oxidation of diverse organic substrates.[1] After binding O_2 gas, the Fe-atom in the active site can traverse through multiple oxidation states thereby generating activated O-O species like superoxo, peroxo, and hydroperoxo while also forming high-valent Iron-Oxo species.[1a-k,1n-r] Therefore oxygenases provide the necessary inspiration to carry out green catalytic transformations under ambient conditions.[1g,1i,2] Although extensive work is being carried out to probe and decipher the mechanistic pathways of these enzymes,[1o,1q,1r,3] direct detection of dioxygen-bound intermediates during catalytic turnover, especially at room temperature remains a challenge.

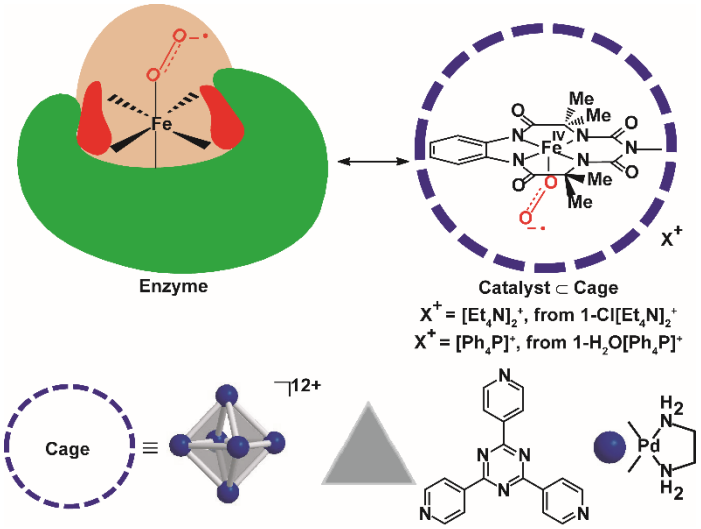

Figure 1. Biomimetic host-encapsulation of Fe(IV)-superoxo species at room temperature. The dioxygen adducts of [Fe^{III}(Cl)-bTAML]$[Et_4N]_2$(1-Cl$[Et_4N]_2$), and [Fe^{III}(OH_2)bTAML]$[Ph_4P]$ (1-$H_2O[Ph_4P]$) were trapped inside an octahedral water-soluble $Pd_6L_4^{12+}$ nanocage; where L= 2,4,6-tri(4-pyridinyl)-1,3,5-triazine, and ethylenediamine holds the Pd^{2+} ion.

Classically bioinorganic chemists have sought to overcome this problem by synthesizing active site mimics that can prove the existence of putative reaction intermediates, and also provide vital insights into the energetics of the catalytic cycle one-step-at-a-time.[2a,2c,2e,2g-i,4] In a variety of oxygenases, the O_2 binding step at the Fe(II) site usually leads to the formation of Fe(III)-$O_2^{\cdot-}$ species.[1a,1c,1g-i,1m] Inspired by the natural enzymes, Collins and coworkers developed a family of Fe(III)-based tera-amido macrocyclic ligand (TAML) catalysts capable of activating O_2 ,and oxidizing organic hydrocarbons.[2a,4-5].[6] SenGupta and co-workers have developed novel biuret tetra-amido macrocyclic ligand (bTAML) catalysts that can stabilize Fe(V)-Oxo intermediate at room temperature while capable of carrying out catalytic water oxidation as well as difficult oxidative organic transformations.[7] In such catalytic schemes involving O_2, the Fe-TAML catalyst dimerizes to generate bridging μ-oxo complexes which are important "on-pathway" intermediates..[1b,1d,1i] However single site activation of O_2 gas that occurs prominently in many monomeric Fe-enzymes can only be mimicked by preventing dimerization which protein active sites successfully manage by building a confinement.

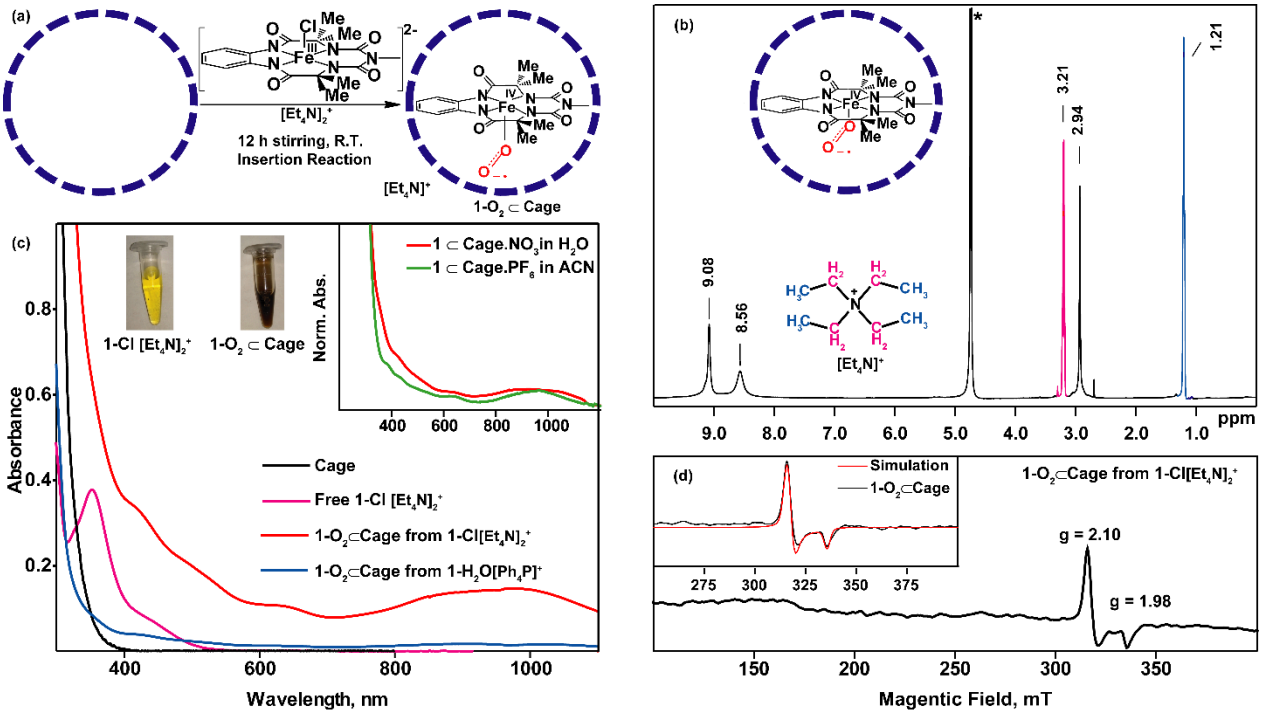

Figure 2. (a) The encapsulation reaction of catalyst **1-Cl** $[Et_4N]_2$, inside $Pd_6L_4^{12+}$ nanocage ; (b) Comparitive absorption spectrum of the cage in water, free **1-Cl** $[Et_4N]_2$ in water, **1-O₂** ⊂ Cage in water after 12 h of reaction, and **1-O₂** ⊂ Cage in water after 6 days of reaction. Inset: comparison of **1-O₂** ⊂ Cage in water, and **1-O₂** ⊂ Cage in acetonitrile after KPF_6 treatment of water sample; (c) ^{1}H-NMR spectrum of **1-O₂** ⊂ Cage recorded in D_2O at 298 K. Cage features are shown as black peaks while from counter ion of **1-Cl** $[Et_4N]_2$, tetraethyl ammonium $[Et_4N]^+$ is shown in pink and blue; (d) EPR spectrum of **1-O₂** ⊂ Cage in water recorded at 93 K. Inset shows EPR spectrum zoomed in the region around g = 2 with the S= ½ simulated spectrum (in red). The simulated spectrum has been vertically offset for visual clarity.

Inspired by protein active sites, supramolecular cavities have been synthesized to host variety of Fe-dioxygen bound intermediates for catalysis.[2i,2k,8] Molecular cages and metal-organic frameworks have shown promise to trap metal-catalysts within their pores thereby protecting them from bimolecular degradation or other side-reactions.[2i,8b,9] Isolated nanocages with size homogeneity can stabilize guest molecules through weak interactions thereby leading to novel chemistry arising from confinement.[9b,9d,10] Here we employ an octahedral water-soluble $Pd_6L_4^{12+}$ nanocage,[11] (see Figure 1) to actively trap an O_2 bound adduct with a fifth-generation [Fe^{III}(Cl)-bTAML] $[Et_4N]_2$ catalyst (**1-Cl** $[Et_4N]_2$) and characterize an elusive yet stable Fe(IV)-$O_2^{\cdot-}$ ([$Fe^{IV}(O_2)$-bTAML] or **1-O₂**) complex inside the nanocage for the first time at room temperature.

The $Pd_6L_4^{12+}$ nanocage with nitrate (NO_3^-) as counter-anion was synthesized using the previously published synthetic route (supporting information, Figure S1).[10e,11] Incarceration of the water soluble catalyst **1-Cl** $[Et_4N]_2$**,** that comprises of negatively charged catalyst species [Fe^{III}(Cl)-bTAML]$^{2-}$ (**1-Cl**) having a counter-cation tetraethylammonium (Et_4N^+), inside the water-soluble $Pd_6L_4^{12+}$ nanocage was carried out at room temperature by stirring in an equimolar concentration of the

nanocage in H_2O for 12 h (see Figure 2a and SI sections 2-4).[9b,9c,10c,10e] The ^{1}H-NMR spectrum of the resulting black color host-guest complex shows broadening of the cage features arising due to the paramagnetic nature of **1-Cl** (S=3/2). The sharp features of the protons at δ 1.21 and 3.21 ppm corresponds to counter-cation Et_4N^+, arises due to its independent solvation in water (Figure 2b and SI Figures S1 and S2).

The black color of **1-O₂** ⊂ Cage solution indicated that the host-guest complex absorbs in the entire visible range, see Figure 2c. Absorption spectra of free **1-Cl** in water has characteristic features at 352 nm corresponding to n→π* transition which is overlapping with MLCT feature on the red edge extending upto ~ 530 nm (Figure 2c).[12] The complex, **1-O₂** ⊂ Cage, on the other hand has an absorption spectrum extended beyond 1100 nm. Interestingly, if the incarceration is carried out under argon atmosphere, the absorption of the complex can simply be explained as a summation of absorption features from the cage and catalyst. The NIR feature seen in regular ambient incarceration does not exist clearly indicating that the chemical form of the catalyst inside the cage under argon is different (SI, Figure S3). A stark difference can also be observed when the samples were prepared in presence of 1-atm of O_2 as compared to ambient O_2 at 1 h (SI, Figure S4). These results unequivocally indicate active participation of O_2 in forming species with NIR absorption, and therefore motivated us to explore the role of molecular oxygen in forming the chemical species trapped inside the cage.

To check if the **1-Cl** indeed went inside the cavity and not trivially solvated in water, we precipitated the host-guest complex by exchanging the nitrate with PF_6^- counter-anion. The **1-O₂** ⊂ Cage.PF_6 complex was soluble in acetonitrile, and indeed retained the incarcerated Fe-catalyst confirmed by recording the steady state absorption spectrum (Figure 2b inset). In addition, we incarcerated a water-insoluble version of the catalyst, compound $(Ph_4P)[Fe^{III}(OH_2)(bTAML)]$ (or **1-H₂O** (Ph_4P)) having a bulkier tetraphenyl-phosphine ligand as counter-cation although with the same catalytic anionic unit. When solid powder of **1-H₂O** (Ph_4P) was stirred with the aqueous solution of the nanocage, the rate of **1-H₂O** incarceration slowed down as expected due to unavailability of the soluble catalyst but in a period of days we observed the expected black color (blue curve Figure 2b and in SI Figures S5 and S6). Incarceration of **1-H₂O** was again confirmed by broadening of the NMR features of the host, and the presence of the proton peaks for the counter cation of **1-H₂O**, i.e. tetraphenyl phosphonium ion (see SI, Figure S7). Based on the stoichiometry of incarceration, retention of structural symmetry of the cage in both salts, and broadening of the cage feature, we conclude that there is one catalytic unit inside every nanocage (Figure S2 and S7). In fact a displacement assay with excess 9-methyl-anthracene (Me-An) added to aqueous solution of **1-O₂** ⊂ Cage was used to confirm the stoichiometry of incarceration (see SI, Figures S8 and S9 for protocol and Figure S10 for UV-Vis characterization). Although Me-An is insoluble in water, it has high affinity for the nanocage[9d,13] due to host-guest CT interactions, and therefore displaces the catalyst from the cage. Using steady state absorption measurements, we observed slow disappearance of the NIR feature associated with **1-O₂** ⊂ Cage with a concomitant increase in the blue-region near 350-400 nm corresponding to Me-An absorption feature[9d,13] (see SI Figures S8-10). We further separated **1-Cl** from this reaction mixture by precipitating Me-An ⊂ Cage by treatment of the reaction mixture with KPF_6. The supernatant which had free compound **1-Cl** was characterized by absorption measurement to confirm that one catalyst per cage was incarcerated (see SI, Figure S8-10). It should be noted that the dioxygen reversibly disengages from the catalyst when forced out of the cavity by Me-An (see SI Figure S10). Such cavity dependent O_2 binding has been previously observed for few Fe(II)-compounds[2i,8a,14] as part of host-guest complexes but for the first time this propensity is observed for an Fe(III) catalyst.

To understand the spin state of **1-O₂** ⊂ Cage, we further carried out steady-state EPR measurements at ~93 K (SI Figure S11). The **1-O₂** ⊂ Cage spectrum was obtained after subtracting the host-guest EPR signal from the empty cage control (Figure 2d, SI Figure S11). The difference spectrum is characterized by an axial g-tensor with features at $g_{xx}=g_{yy}= 2.102$ and $g_z=1.985$ as obtained by simulating the EPR spectrum corresponding to S = ½ species (Figure 2d, and SI Figure S12). This spectrum is in direct contrast to the S = 3/2 spin state spectrum (SI Figure S11) reported for the free catalyst **1-Cl** in both solid state and a derivative of catalyst **1-Cl**$[Et_4N]_2$ in acetonitrile.[7d,12] However, Fe(III)-bTAML can be S = ½ species if we imply an O_2 bound adduct leading to formation of Fe(IV)-$O_2^{\cdot-}$. To chemically test this hypothesis, Fe(IV)-bTAML salt was prepared by chemically oxidizing the Fe(III)-version with $(NH_4)_2Ce(NO_3)_6$ (SI Figure S13).[70] Upon reacting it with KO_2 at -40 ºC, we obtain an S = ½ EPR signal mirroring what was obtained for **1-O₂** ⊂ Cage (Figure S14 in SI). Therefore based on our results, we have assigned the cage entrapped species as a monomeric Fe(IV)-$O_2^{\cdot-}$ superoxide species stabilized inside the water-soluble cationic $Pd_6L_4^{12+}$ host. The obtained spin state S = ½ combined with the clear signature of an NIR absorption feature and reversibility in O_2 binding strongly support the assignment. To the best of our knowledge Fe(IV)-$O_2^{\cdot-}$ superoxide species has never been detected in any catalytic cycle involving O_2 activation.

Collins and coworkers recently reported that paramagnetic Fe-TAML complexes inside reverse micelles can react with O_2, and thus form an absorption band extended to NIR region indicative of Fe(IV)-based MLCT transitions.[6b] Due to a large distribution in the micelle size ranging from 1-5 nanometers[15], they observed multiple species ranging from unreacted Fe(III) catalyst, Fe(III)–Fe(IV), and Fe(IV)–Fe(IV) μ-oxo dimers.[6b] The dimers were formed upon an irreversible reaction with O_2, and could only revert back to Fe(III) state after one-electron reduction.[6b] The Fe(III)–Fe(IV) μ-oxo dimer was found to be S = ½ while the $[\{(bTAML)Fe^{IV}\}_2$-μ-Oxo$]^{2-}$ species was EPR-silent. SenGupta and coworkers showed that the diamagnetic dimer formed by **1-Cl**$[Et_4N]_2$ after getting oxidized by on-electron oxidant also shows the NIR absorption feature indicative of Fe(IV) state.[7a,7c,7d] In summary, our observations of reversible aerial oxidation of the Fe(III) catalyst yielding a S = ½

species inside a ~2 nm nanocage is a novel observation, and indicates homogenous population of monomeric Fe(IV)-superoxo species trapped inside a cavity at room temperature.

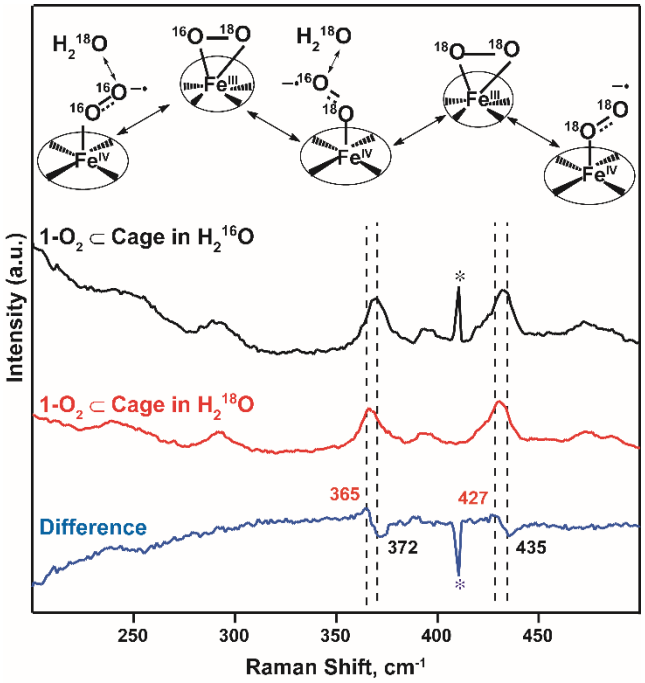

Figure 3. Resonance Raman spectra of **1-O_2** ⊂ Cage prepared in $H_2{}^{16}O$ (in black), **1-O_2** ⊂ Cage prepared in $H_2{}^{18}O$ (in red) and the normalized difference spectra. The asterisks depict cosmic artifacts during data collection.

The unique reactivity of the cavity-trapped Fe(IV)-superoxo species with solvent water was used to determine its existence. The rapid $^{18}O/^{16}O$-exchange equilibrium driven by water attack through protonation of the distal O-atom in superoxide leads to ^{18}O-isotopic enrichment in the O-O bond from $H_2{}^{18}O$ (Figure 3). The fast isomerization of the end-on peroxo with its side-on binding configuration allows for both O-atoms to be enriched in a facile fashion. We recorded the vibrational resonance Raman spectrum of **1-O_2** ⊂ Cage in both $H_2{}^{16}O$ and $H_2{}^{18}O$ to unequivocally assign the incarcerated Fe(IV)-superoxo species. The Raman vibrations of the catalyst are enunciated in the range of 250 to 1200 cm^{-1} (SI Figure S15). We observe low frequency vibrational features corresponding to Fe(IV)-O_2 stretch (side-on) at ~ 433 cm^{-1} and Fe-OO bend (end-on) at ~ 370 cm^{-1} in $H_2{}^{16}O$ (Figure 3) which are slightly shifted compared to reported Fe(III)-superoxo species.[16] Interestingly these vibrational features are red-shifted further by 7-8 cm^{-1} for the spectrum recorded in $H_2{}^{18}O$ as illustrated by the difference spectra in blue (Figure 3, SI Figure S15, Table ST1). It is important to note that sharp cage features at 1042 and 1062 cm^{-1} assigned to nitrate N-O stretch and NH_2 wagging of the ethyelenediamine moeity[14] respectively, is resonantly affected by solvent exchange thereby indicating altered H-bonding in $H_2{}^{18}O$. These features however mask the weak O-O stretch feature at 1086 cm^{-1} although the isotope sensitivity can be uncovered by subtracting the dominant cage peaks carefully (SI Figure S15).[17] We also see the side-on O-O stretch feature coupled to ligand vibrations at 697 cm^{-1} disappear with ^{18}O-isotope enrichment similar to that observed for Fe(III)-superoxo complex for TPP.[16c] We see isotope shifts in all these features and other weaker signals between 600-900 cm^{-1} under the constraint of the signal to noise, clearly enunciating the presence of an Fe(IV)-superoxo species. Indeed to confirm separately this exchange, we also carried out $^{16}O_2$ and $^{18}O_2$ labelling experiments, which did not show any shifts as expected since the label got washed away in the background of 55 M $H_2{}^{16}O$ (SI Figure S16). Overall our Raman measurements unequivocally prove that indeed a labile O-O bond is present which highlights the superoxide state of O_2 bound to the Fe(IV) core.

In conclusion, we have used host-guest complexation as a facile methodology to isolate and characterize a novel yet stable Fe(IV)-O_2^- species at room temperature for the first time. We believe that the Fe(IV)-superoxo species is a precursor to the previously reported Fe(III)–Fe(IV) μ-oxo dimers commonly observed during catalytic oxidation of substrates with Fe(III)-TAML catalysts that activate O_2 gas.[6b,18] The hydrophobic confinement of the water soluble nanocage highlights the importance of the host structure and specific water interactions[10e,13] to stabilize extra charge on oxygen thereby allowing detection of a high-valent intermediate. The cavity size also becomes important to tune for ensuring a homogenous population of high-valent Fe-oxy adducts while preventing dimerization reactions. We therefore envision that trapping

intermediates in molecular confinement by choosing optimal size and electronic nature of the host[19] should allow for a universal scheme of probing reactive intermediates without compromising the catalytic efficiency.

ASSOCIATED CONTENT

Details of synthesis, characterization and additional data are provided. This material is available free of charge via the Internet at **http://pubs.acs.org**.

Corresponding Author

* **Email: dasgupta@tifr.res.in**

Present Addresses

¶AMOLF, Science Park 104, 1098 XG Amsterdam, The Netherlands.

ACKNOWLEDGMENT

The authors acknowledge the scientific discussions with Dr. A. Das, Dr. K. Vijayalakshmi, Dr. A. Jha and Dr. P. Roy. Special thanks to Dr. A. Das, Ms. S. Paul and Mr. A. Ghosh for help in editing the manuscript. JD thanks TIFR and the Department of Atomic Energy (DAE), Government of India, for funds under Project No. 12-R&D-TFR-5.10-0100.

REFERENCES

(1) (a) Meunier, B.; de Visser, S. P.; Shaik, S. Mechanism of Oxidation Reactions Catalyzed by Cytochrome P450 Enzymes *Chemical Reviews* **2004**, *104*, 3947. (b) Kovaleva, E. G.; Neibergall, M. B.; Chakrabarty, S.; Lipscomb, J. D. Finding Intermediates in the O2 Activation Pathways of Non-Heme Iron Oxygenases *Accounts of Chemical Research* **2007**, *40*, 475. (c) Krebs, C.; Galonić Fujimori, D.; Walsh, C. T.; Bollinger, J. M. Non-Heme Fe(IV)–Oxo Intermediates *Accounts of Chemical Research* **2007**, *40*, 484. (d) Murray, L. J.; Lippard, S. J. Substrate Trafficking and Dioxygen Activation in Bacterial Multicomponent Monooxygenases *Accounts of Chemical Research* **2007**, *40*, 466. (e) Watanabe, Y.; Nakajima, H.; Ueno, T. Reactivities of Oxo and Peroxo Intermediates Studied by Hemoprotein Mutants *Accounts of Chemical Research* **2007**, *40*, 554. (f) Abu-Omar, M. M.; Loaiza, A.; Hontzeas, N. Reaction Mechanisms of Mononuclear Non-Heme Iron Oxygenases *Chemical Reviews* **2005**, *105*, 2227. (g) Costas, M.; Mehn, M. P.; Jensen, M. P.; Que, L. Dioxygen Activation at Mononuclear Nonheme Iron Active Sites: Enzymes, Models, and Intermediates *Chemical Reviews* **2004**, *104*, 939. (h) Denisov, I. G.; Makris, T. M.; Sligar, S. G.; Schlichting, I. Structure and Chemistry of Cytochrome P450 *Chemical Reviews* **2005**, *105*, 2253. (i) Feig, A. L.; Lippard, S. J. Reactions of Non-Heme Iron(II) Centers with Dioxygen in Biology and Chemistry *Chemical Reviews* **1994**, *94*, 759. (j) Bollinger Jr, J. M.; Krebs, C. Stalking intermediates in oxygen activation by iron enzymes: Motivation and method *Journal of Inorganic Biochemistry* **2006**, *100*, 586. (k) Fontecilla-Camps, J. C.; Amara, P.; Cavazza, C.; Nicolet, Y.; Volbeda, A. Structure–function relationships of anaerobic gas-processing metalloenzymes *Nature* **2009**, *460*, 814. (l) Solomon, E. I.; Goudarzi, S.; Sutherlin, K. D. O2 Activation by Non-Heme Iron Enzymes *Biochemistry* **2016**, *55*, 6363. (m) Solomon, E. I.; Light, K. M.; Liu, L. V.; Srnec, M.; Wong, S. D. Geometric and Electronic Structure Contributions to Function in Non-heme Iron Enzymes *Accounts of Chemical Research* **2013**, *46*, 2725. (n) Balasubramanian, R.; Rosenzweig, A. C. Structural and Mechanistic Insights into Methane Oxidation by Particulate Methane Monooxygenase *Accounts of Chemical Research* **2007**, *40*, 573. (o) Orville, A. M.; Lipscomb, J. D.; Ohlendorf, D. H. Crystal Structures of Substrate and Substrate Analog Complexes of Protocatechuate 3,4-Dioxygenase: Endogenous Fe3+ Ligand Displacement in Response to Substrate Binding *Biochemistry* **1997**, *36*, 10052. (p) van der Donk, W. A.; Krebs, C.; Bollinger Jr, J. M. Substrate activation by iron superoxo intermediates *Current Opinion in Structural Biology* **2010**, *20*, 673. (q) Davydov, R.; Kofman, V.; Fujii, H.; Yoshida, T.; Ikeda-Saito, M.; Hoffman, B. M. Catalytic Mechanism of Heme Oxygenase through EPR and ENDOR of Cryoreduced Oxy-Heme Oxygenase and Its Asp 140 Mutants *Journal of the American Chemical Society* **2002**, *124*, 1798. (r) Davydov, R.; Perera, R.; Jin, S.; Yang, T.-C.; Bryson, T. A.; Sono, M.; Dawson, J. H.; Hoffman, B. M. Substrate Modulation of the Properties and Reactivity of the Oxy-Ferrous and Hydroperoxo-Ferric Intermediates of Cytochrome P450cam As Shown by Cryoreduction-EPR/ENDOR Spectroscopy *Journal of the American Chemical Society* **2005**, *127*, 1403.
(2) (a) Collins, T. J. Designing Ligands for Oxidizing Complexes *Accounts of Chemical Research* **1994**, *27*, 279. (b) Korendovych, I. V.; Kryatov, S. V.; Rybak-Akimova, E. V. Dioxygen Activation at Non-Heme Iron: Insights from Rapid Kinetic Studies *Accounts of Chemical Research* **2007**, *40*, 510. (c) Nam, W. Synthetic Mononuclear Nonheme Iron–Oxygen Intermediates *Accounts of Chemical Research* **2015**, *48*, 2415. (d) Nam, W.; Lee, Y.-M.; Fukuzumi, S. Tuning Reactivity and Mechanism in Oxidation Reactions by Mononuclear Nonheme Iron(IV)-Oxo Complexes *Accounts of Chemical Research* **2014**, *47*, 1146. (e) Oloo, W. N.; Que, L. Bioinspired Nonheme Iron Catalysts for C–H and C═C Bond Oxidation: Insights into the Nature of the Metal-Based Oxidants *Accounts of Chemical Research* **2015**, *48*, 2612. (f) Que, L. The Road to Non-Heme Oxoferryls and Beyond † *Accounts of Chemical Research* **2007**, *40*, 493. (g) Sallmann, M.; Limberg, C. Utilizing the Trispyrazolyl Borate Ligand for the Mimicking of O2-Activating Mononuclear Nonheme Iron Enzymes *Accounts of Chemical Research* **2015**, *48*, 2734. (h) Momenteau, M.; Reed, C. A. Synthetic Heme-Dioxygen Complexes *Chemical Reviews* **1994**, *94*, 659. (i) Rebilly, J.-N.; Colasson, B.; Bistri, O.; Over, D.; Reinaud, O. Biomimetic cavity-based metal complexes *Chemical Society Reviews* **2015**, *44*, 467. (j) de Visser, S. P.; Rohde, J.-U.; Lee, Y.-M.; Cho, J.; Nam, W. Intrinsic properties and reactivities of mononuclear nonheme iron–oxygen complexes bearing the tetramethylcyclam ligand *Coordination Chemistry Reviews* **2013**, *257*, 381. (k) Snyder, B. E. R.; Bols, M. L.; Schoonheydt, R. A.; Sels, B. F.; Solomon, E. I. Iron and Copper Active Sites in Zeolites and Their Correlation to Metalloenzymes *Chemical Reviews* **2018**, *118*, 2718.

(3) (a) Davydov, R.; Satterlee, J. D.; Fujii, H.; Sauer-Masarwa, A.; Busch, D. H.; Hoffman, B. M. A Superoxo-Ferrous State in a Reduced Oxy-Ferrous Hemoprotein and Model Compounds *Journal of the American Chemical Society* **2003**, *125*, 16340. (b) Davydov, R. M.; Yoshida, T.; Ikeda-Saito, M.; Hoffman, B. M. Hydroperoxy-Heme Oxygenase Generated by Cryoreduction Catalyzes the Formation of α-meso-Hydroxyheme as Detected by EPR and ENDOR *Journal of the American Chemical Society* **1999**, *121*, 10656. (c) Garcia-Serres, R.; Davydov, R. M.; Matsui, T.; Ikeda-Saito, M.; Hoffman, B. M.; Huynh, B. H. Distinct Reaction Pathways Followed upon Reduction of Oxy-Heme Oxygenase and Oxy-Myoglobin as Characterized by Mössbauer Spectroscopy *Journal of the American Chemical Society* **2007**, *129*, 1402. (d) Ibrahim, M.; Denisov, I. G.; Makris, T. M.; Kincaid, J. R.; Sligar, S. G. Resonance Raman Spectroscopic Studies of Hydroperoxo-Myoglobin at Cryogenic Temperatures *Journal of the American Chemical Society* **2003**, *125*, 13714. (e) Price, J. C.; Barr, E. W.; Glass, T. E.; Krebs, C.; Bollinger, J. M. Evidence for Hydrogen Abstraction from C1 of Taurine by the High-Spin Fe(IV) Intermediate Detected during Oxygen Activation by Taurine:α-Ketoglutarate Dioxygenase (TauD) *Journal of the American Chemical Society* **2003**, *125*, 13008. (f) Galonic, D. P.; Barr, E. W.; Walsh, C. T.; Bollinger, J. M.; Krebs, C. Two interconverting Fe(IV) intermediates in aliphatic chlorination by the halogenase CytC3 *Nat Chem Biol* **2007**, *3*, 113. (g) Solomon, E. I.; Decker, A.; Lehnert, N. Non-heme iron enzymes: Contrasts to heme catalysis *Proceedings of the National Academy of Sciences* **2003**, *100*, 3589. (h) Karlsson, A.; Parales, J. V.; Parales, R. E.; Gibson, D. T.; Eklund, H.; Ramaswamy, S. Crystal Structure of Naphthalene Dioxygenase: Side-on Binding of Dioxygen to Iron *Science* **2003**, *299*, 1039. (i) Kovaleva, E. G.; Lipscomb, J. D. Crystal Structures of Fe2+ Dioxygenase Superoxo, Alkylperoxo, and Bound Product Intermediates *Science* **2007**, *316*, 453. (j) Mara, M. W.; Hadt, R. G.; Reinhard, M. E.; Kroll, T.; Lim, H.; Hartsock, R. W.; Alonso-Mori, R.; Chollet, M.; Glownia, J. M.; Nelson, S.; Sokaras, D.; Kunnus, K.; Hodgson, K. O.; Hedman, B.; Bergmann, U.; Gaffney, K. J.; Solomon, E. I. Metalloprotein entatic control of ligand-metal bonds quantified by ultrafast x-ray spectroscopy *Science* **2017**, *356*, 1276.

(4) Collins, T. J. TAML Oxidant Activators: A New Approach to the Activation of Hydrogen Peroxide for Environmentally Significant Problems *Accounts of Chemical Research* **2002**, *35*, 782.

(5) Chanda, A.; Popescu, D.-L.; de Oliveira, F. T.; Bominaar, E. L.; Ryabov, A. D.; Münck, E.; Collins, T. J. High-valent iron complexes with tetraamido macrocyclic ligands: Structures, Mössbauer spectroscopy, and DFT calculations *Journal of Inorganic Biochemistry* **2006**, *100*, 606.

(6) (a) Ghosh, A.; Tiago de Oliveira, F.; Yano, T.; Nishioka, T.; Beach, E. S.; Kinoshita, I.; Münck, E.; Ryabov, A. D.; Horwitz, C. P.; Collins, T. J. Catalytically Active μ-Oxodiiron(IV) Oxidants from Iron(III) and Dioxygen *Journal of the American Chemical Society* **2005**, *127*, 2505. (b) Tang, L. L.; Gunderson, W. A.; Weitz, A. C.; Hendrich, M. P.; Ryabov, A. D.; Collins, T. J. Activation of Dioxygen by a TAML Activator in Reverse Micelles: Characterization of an FeIIIFeIV Dimer and Associated Catalytic Chemistry *Journal of the American Chemical Society* **2015**, *137*, 9704.

(7) (a) Singh, K. K.; Tiwari, M. k.; Dhar, B. B.; Vanka, K.; Sen Gupta, S. Mechanism of Oxygen Atom Transfer from FeV(O) to Olefins at Room Temperature *Inorganic Chemistry* **2015**, *54*, 6112. (b) Singh, K. K.; Tiwari, M. k.; Ghosh, M.; Panda, C.; Weitz, A.; Hendrich, M. P.; Dhar, B. B.; Vanka, K.; Sen Gupta, S. Tuning the Reactivity of FeV(O) toward C–H Bonds at Room Temperature: Effect of Water *Inorganic Chemistry* **2015**, *54*, 1535. (c) Ghosh, M.; Singh, K. K.; Panda, C.; Weitz, A.; Hendrich, M. P.; Collins, T. J.; Dhar, B. B.; Sen Gupta, S. Formation of a Room Temperature Stable FeV(O) Complex: Reactivity Toward Unactivated C–H Bonds *Journal of the American Chemical Society* **2014**, *136*, 9524. (d) Panda, C.; Debgupta, J.; Díaz Díaz, D.; Singh, K. K.; Sen Gupta, S.; Dhar, B. B. Homogeneous Photochemical Water Oxidation by Biuret-Modified Fe-TAML: Evidence of FeV(O) Intermediate *Journal of the American Chemical Society* **2014**, *136*, 12273.

(8) (a) Kano, K.; Kitagishi, H.; Dagallier, C.; Kodera, M.; Matsuo, T.; Hayashi, T.; Hisaeda, Y.; Hirota, S. Iron Porphyrin−Cyclodextrin Supramolecular Complex as a Functional Model of Myoglobin in Aqueous Solution *Inorganic Chemistry* **2006**, *45*, 4448. (b) Anderson, J. S.; Gallagher, A. T.; Mason, J. A.; Harris, T. D. A Five-Coordinate Heme Dioxygen Adduct Isolated within a Metal–Organic Framework *Journal of the American Chemical Society* **2014**, *136*, 16489.

(9) (a) Horiuchi, S.; Murase, T.; Fujita, M. Noncovalent Trapping and Stabilization of Dinuclear Ruthenium Complexes within a Coordination Cage *Journal of the American Chemical Society* **2011**, *133*, 12445. (b) Kawano, M.; Kobayashi, Y.; Ozeki, T.; Fujita, M. Direct Crystallographic Observation of a Coordinatively Unsaturated Transition-Metal Complex in situ Generated within a Self-Assembled Cage *Journal of the American Chemical Society* **2006**, *128*, 6558. (c) Kohyama, Y.; Murase, T.; Fujita, M. Metal–Organic Proximity in a Synthetic Pocket *Journal of the American Chemical Society* **2014**, *136*, 2966. (d) Das, A.; Mandal, I.; Venkatramani, R.; Dasgupta, J. Ultrafast photoactivation of C─H bonds inside water-soluble nanocages *Science Advances* **2019**, *5*, eaav4806. (e) Nepal, B.; Das, S. Sustained Water Oxidation by a Catalyst Cage-Isolated in a Metal–Organic Framework *Angewandte Chemie International Edition* **2013**, *52*, 7224.

(10) (a) He, Q.-T.; Li, X.-P.; Chen, L.-F.; Zhang, L.; Wang, W.; Su, C.-Y. Nanosized Coordination Cages Incorporating Multiple Cu(I) Reactive Sites: Host–Guest Modulated Catalytic Activity *ACS Catalysis* **2013**, *3*, 1. (b) Guo, J.; Xu, Y.-W.; Li, K.; Xiao, L.-M.; Chen, S.; Wu, K.; Chen, X.-D.; Fan, Y.-Z.; Liu, J.-M.; Su, C.-Y. Regio- and Enantioselective Photodimerization within the Confined Space of a Homochiral Ruthenium/Palladium Heterometallic Coordination Cage *Angewandte Chemie International Edition* **2017**, *56*, 3852. (c) Horiuchi, S.; Murase, T.; Fujita, M. A Remarkable Organometallic Transformation on a Cage-Incarcerated Dinuclear Ruthenium Complex *Angewandte Chemie International Edition* **2012**, *51*, 12029. (d) Smulders, M. M. J.; Nitschke, J. R. Supramolecular control over Diels-Alder reactivity by encapsulation and competitive displacement *Chemical Science* **2012**, *3*, 785. (e) Gera, R.; Das, A.; Jha, A.; Dasgupta, J. Light-Induced Proton-Coupled Electron Transfer Inside a Nanocage *Journal of the American Chemical Society* **2014**, *136*, 15909. (f) Omagari, T.; Suzuki, A.; Akita, M.; Yoshizawa, M. Efficient Catalytic Epoxidation in Water by Axial N-Ligand-Free Mn-Porphyrins within a Micellar Capsule *Journal of the American Chemical Society* **2016**, *138*, 499. (g) Gera, R.; Meloni, S. L.; Anna, J. M. Unraveling Confined Dynamics of Guests

Trapped in Self-Assembled Pd6L4 Nanocages by Ultrafast Mid-IR Polarization-Dependent Spectroscopy *The Journal of Physical Chemistry Letters* **2019**, *10*, 413.
(11) Fujita, M.; Oguro, D.; Miyazawa, M.; Oka, H.; Yamaguchi, K.; Ogura, K. Self-assembly of ten molecules into nanometre-sized organic host frameworks *Nature* **1995**, *378*, 469.
(12) Panda, C.; Ghosh, M.; Panda, T.; Banerjee, R.; Sen Gupta, S. Fe(iii) complex of biuret-amide based macrocyclic ligand as peroxidase enzyme mimic *Chemical Communications* **2011**, *47*, 8016.
(13) Das, A.; Jha, A.; Gera, R.; Dasgupta, J. Photoinduced Charge Transfer State Probes the Dynamic Water Interaction with Metal–Organic Nanocages *The Journal of Physical Chemistry C* **2015**, *119*, 21234.
(14) Kano, K.; Kitagishi, H.; Kodera, M.; Hirota, S. Dioxygen Binding to a Simple Myoglobin Model in Aqueous Solution *Angewandte Chemie International Edition* **2005**, *44*, 435.
(15) Amararene, A.; Gindre, M.; Le Huérou, J. Y.; Urbach, W.; Valdez, D.; Waks, M. Adiabatic compressibility of AOT [sodium bis(2-ethylhexyl)sulfosuccinate] reverse micelles: Analysis of a simple model based on micellar size and volumetric measurements *Physical Review E* **2000**, *61*, 682.
(16) (a) Gordon, J. B.; Vilbert, A. C.; Siegler, M. A.; Lancaster, K. M.; Moënne-Loccoz, P.; Goldberg, D. P. A Nonheme Thiolate-Ligated Cobalt Superoxo Complex: Synthesis and Spectroscopic Characterization, Computational Studies, and Hydrogen Atom Abstraction Reactivity *Journal of the American Chemical Society* **2019**, *141*, 3641. (b) Wasser, I. M.; Huang, H.-w.; Moënne-Loccoz, P.; Karlin, K. D. Heme/Non-Heme Diiron(II) Complexes and O2, CO, and NO Adducts as Reduced and Substrate-Bound Models for the Active Site of Bacterial Nitric Oxide Reductase *Journal of the American Chemical Society* **2005**, *127*, 3310. (c) Proniewicz, L. M.; Paeng, I. R.; Nakamoto, K. Resonance Raman spectra of two isomeric dioxygen adducts of iron(II) porphyrins and .pi.-cation radical and nonradical oxoferryl porphyrins produced in dioxygen matrixes: simultaneous observation of more than seven oxygen isotope sensitive bands *Journal of the American Chemical Society* **1991**, *113*, 3294. (d) Vogel, K. M.; Kozlowski, P. M.; Zgierski, M. Z.; Spiro, T. G. Determinants of the FeXO (X = C, N, O) Vibrational Frequencies in Heme Adducts from Experiment and Density Functional Theory *Journal of the American Chemical Society* **1999**, *121*, 9915.
(17) Lin, Y.-H.; Kutin, Y.; van Gastel, M.; Bill, E.; Schnegg, A.; Ye, S.; Lee, W.-Z. A Manganese(IV)-Hydroperoxo Intermediate Generated by Protonation of the Corresponding Manganese(III)-Superoxo Complex *Journal of the American Chemical Society* **2020**, *142*, 10255.
(18) Singh, K. K.; Sen Gupta, S. Reductive activation of O2 by a bioinspired Fe complex for catalytic epoxidation reactions *Chemical Communications* **2017**, *53*, 5914.
(19) Serrano-Plana, J.; Rumo, C.; Rebelein, J. G.; Peterson, R. L.; Barnet, M.; Ward, T. R. Enantioselective Hydroxylation of Benzylic C(sp3)–H Bonds by an Artificial Iron Hydroxylase Based on the Biotin–Streptavidin Technology *Journal of the American Chemical Society* **2020**, *142*, 10617.

SYNOPSIS TOC.

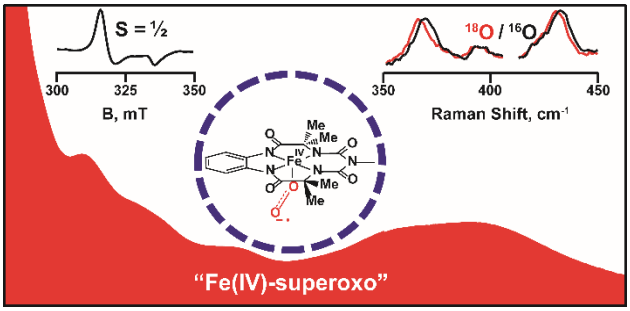

Supporting Information

Trapping an Elusive Fe(IV)-superoxo Intermediate Inside -a Self-Assembled Nanocage at Room Temperature

Rahul Gera,[†§], Kundan K. Singh,[‡] Sayam Sen Gupta,[‡] and Jyotishman Dasgupta[†*]

[†]Department of Chemical Sciences, Tata Institute of Fundamental Research, Mumbai 400005, India.

[‡]Chemical Engineering Division, CSIR-National Chemical Laboratory, Dr. Homi Bhabha Road, Pune, Maharashtra 411008, India

*Email: dasgupta@tifr.res.in

Contents:

Supplementary Figures:

Supplementary Table:

1. Materials and Methods:

Solvents and reagents were purchased from TCI Co., Ltd., S.D. Fine Chemicals and Sigma-Aldrich Co. D_2O was acquired from Sigma-Aldrich Co, Inc. and used as supplied for the reactions and NMR measurements.

NMR Measurements:

^1H spectra were recorded on Bruker (500 MHz) and Varian (600 MHz) spectrometer.

Steady State Absorption Measurements:

Steady state absorption was recorded on JASCO V-670 spectrophotometer

Steady state Electron Paramagnetic Resonance (EPR) spectroscopy

Steady state EPR measurements were carried out on a BRUKER EMX Micro X-band spectrometer. These measurements were carried out at ~ 90 K. Temperature of the EPR cavity was maintained by flushing liquid nitrogen from a reservoir to an insert in the cavity. The insert has a thermocouple as a temperature sensor and the EPR measurements were performed inside the same insert. The operating frequency of the spectrometer is 9.32 GHz. Operating microwave power of the spectrometer is 0.2 mW, with modulation amplitude of 1 Gauss and modulation frequency of 100 kHz. Simulations of EPR spectra of $\mathbf{1} \subset$ Cage performed for a single spin S = ½ using commercially available software WIN-EPR SimFonia.

Resonance Raman spectroscopy

Raman measurements were performed on an Alpha 300R confocal Raman microscope, WITec Gmbh, Ulm (Germany). These measurements were performed using a 532 nm laser as the excitation source generated from solid state frequency-doubled DPSS Nd:YAG laser (WITec). The backscattered light was channeled by a lens-based ultrahigh throughput spectrometer (UHTS300) through a 100 μm optical fiber onto a grating of 1800 grooves/mm coupled to a back-illuminated CCD

camera. Spectral resolution of the spectrograph was ~ 2 cm^{-1}. Laser was focused into the sample using a 10X objective. The sample was flowed to prevent from photobleaching through a quartz cuvette of 0.5 mm thickness.

2. Synthesis of the cationic (Pd_6L_4) cage:

Cage 1 was prepared according to M. Fujita et al. Nature 1995, 378, 469 to get Pd_6L_4 $(NO_3)_{12}$ complex. To a solution of $Pd(en)(ONO_2)_2$ (2.5 g, 8.62 mmol) in H_2O, we added 1.8 g (5.75 mmol) of 2,4,6-tri(4-pyridyl)-1,3,5-triazine was added. The obtained suspension was refluxed at 80 °C for 6 hours. Insoluble material was filtered using Whatman filter paper, and the clear solution was evaporated to give 1.07 g (70%) of 1 as a pale white powder: ^{1}H NMR (600MHz, D_2O, 298 K): δ 9.00 (d, 24H, pyridine-α), 8.51 (d, 24H, pyridine-β), 2.85 (s, 24H).

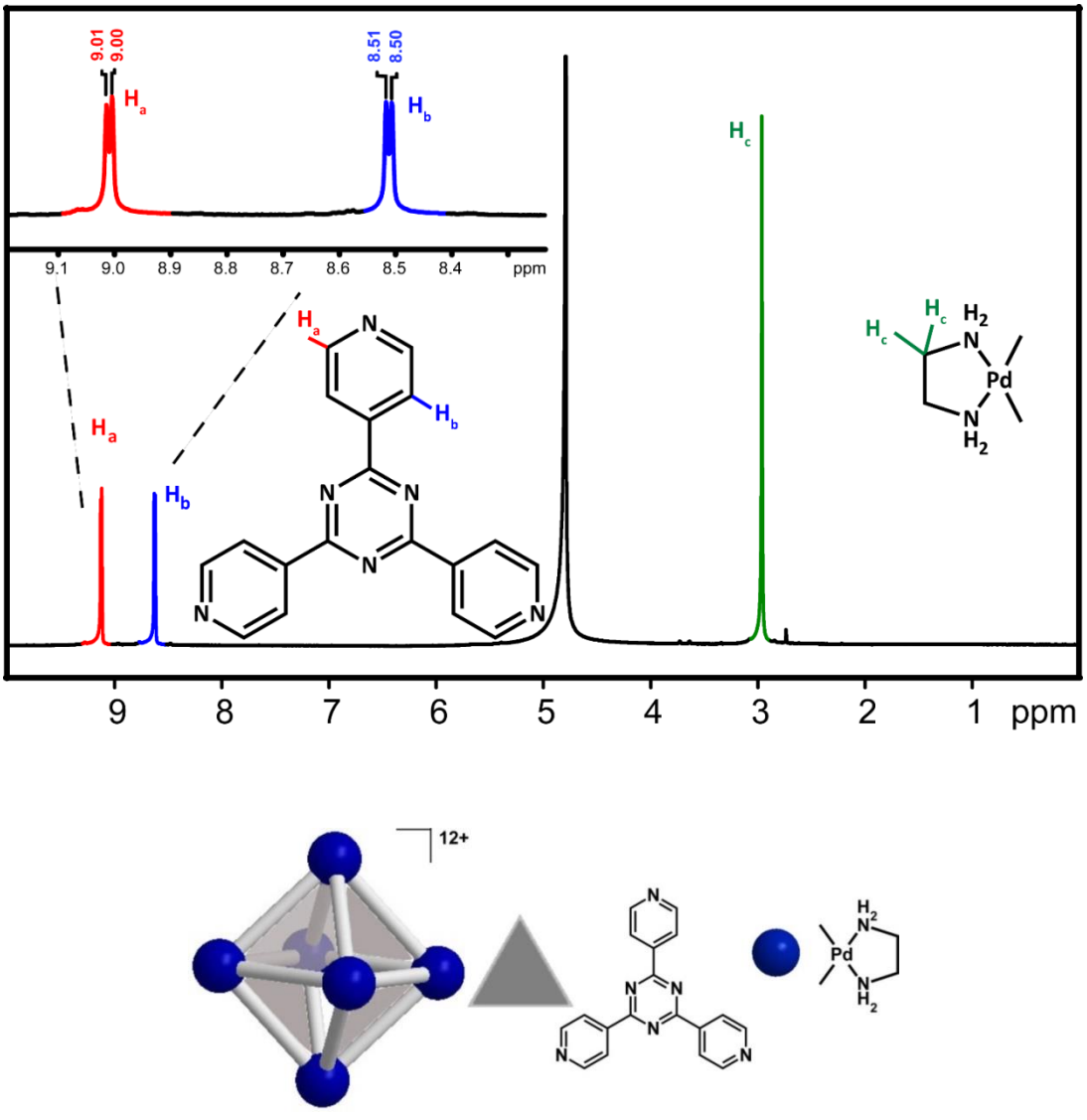

Figure S1. ^{1}H NMR spectra (600 MHz, 298 K) of Cage.

3. Synthesis of the inclusion complex 1-O_2 ⊂ cage:

1.4 mg of **1-Cl**$[Et_4N]_2$ catalyst was stirred for 12 h in a 1 ml solution of 2 mM Cage so as to maintain 1:1 catalyst:cage ratio in D_2O. The colorless cage solution changes to black overtime. The solution was filtered through a 0.45 μ filter. Characterization of the reaction mixture was done through NMR and UV visible absorption. Samples were taken for further measurements only when characterized through proton NMR and steady state absorption. ^{1}H NMR (500 MHz, D_2O, 298 K): δ 9.08 (d, pyridine-α, Cage), 8.56 (d, pyridine-β, Cage), δ 3.21 (q, -CH_2-, Et_4N^+), δ 2.94 (s, N-CH2CH2-N, Cage), δ 1.21 (t, CH_3-, Et_4N^+).

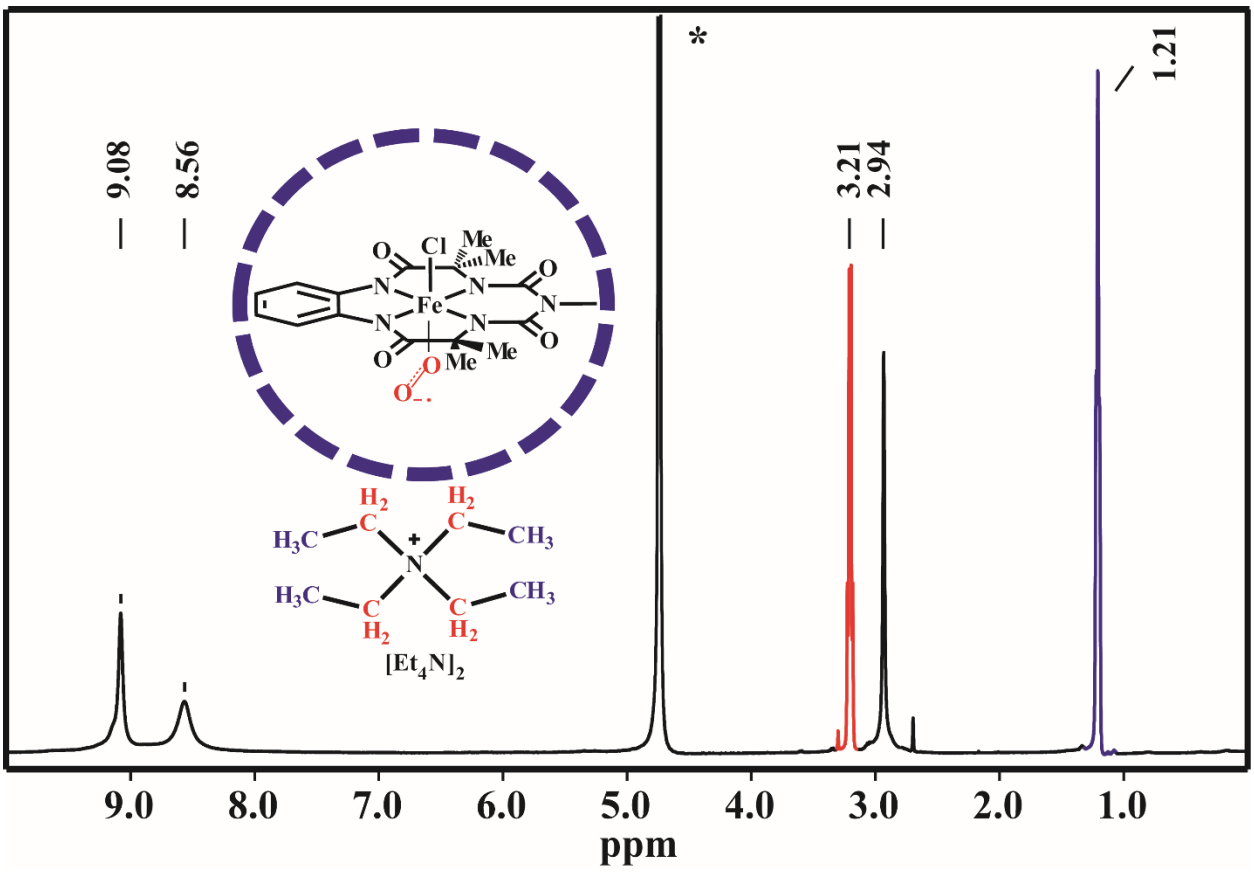

Figure S2. ^{1}H NMR of inclusion complex **1-O_2** ⊂ Cage (600 MHz, 298 K). The features from catalyst were absent, counter cation of the catalyst appeared at δ 3.21 ppm as quartet (in red) and δ 1.21 ppm as triplet (in blue). 2,4,6-trispyridyltriazine feature in the Cage 1 at δ 9.08 ppm and δ 8.56 ppm are broadened along with the features from ethylenediamine at δ 2.94 ppm.

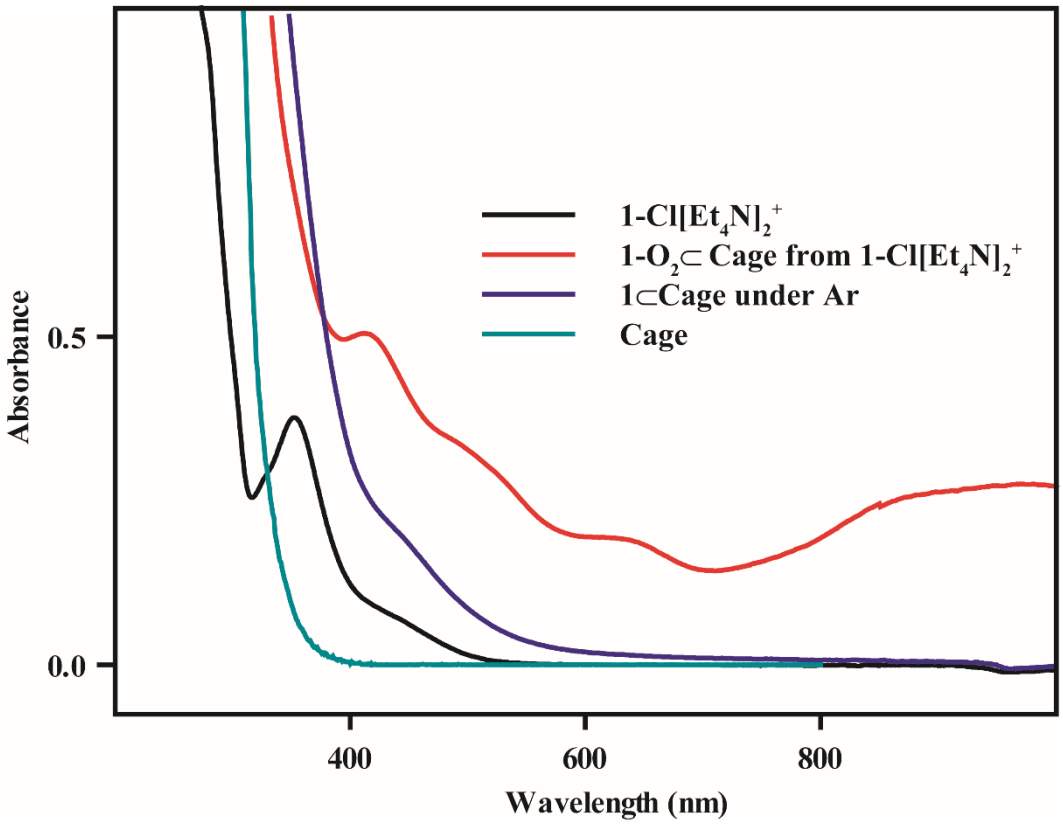

Figure S3. Steady state absorption spectra of pure empty cage (80 μM), the free **1-Cl**$[\boldsymbol{Et_4N}]_2$ complex in water and the host-guest complex (200 μM in water) in both ambient conditions and under Argon atmosphere. The color traces are indeed as follows: Cage (in cyan), **1-Cl**$[\boldsymbol{Et_4N}]_2$ (in black), **1-O$_2$** ⊂ Cage under ambient conditions (in red) and **1** ⊂ Cage under argon atmosphere (in blue).

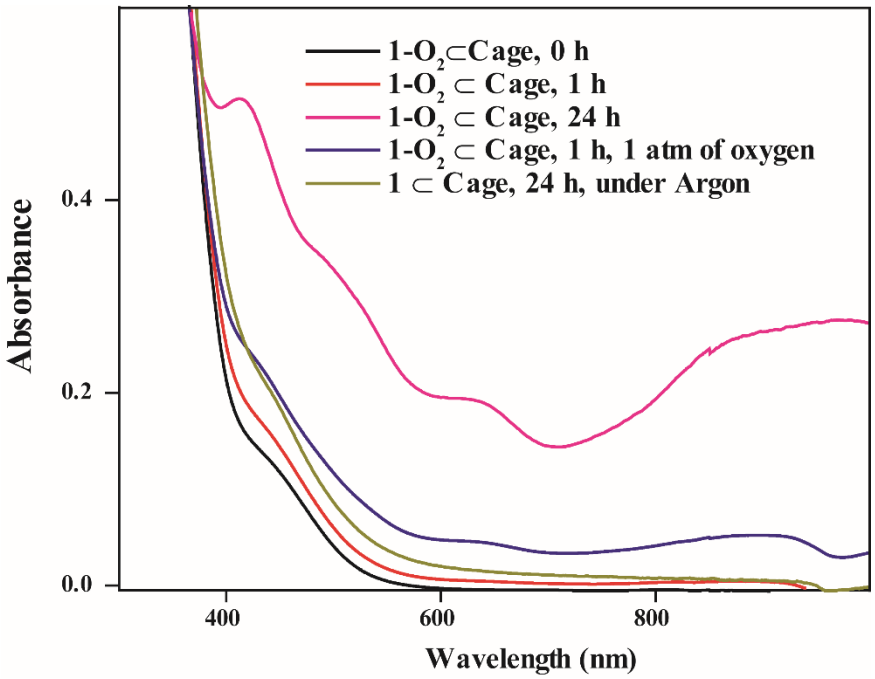

Figure S4. Comparative steady state absorption spectra for incarceration of complex **1-Cl**$[\boldsymbol{Et_4N}]_2$ inside Cage (200 μM) at different times, and also under varying oxygen pressures.

4. Insertion with water insoluble catalyst to form 1-O_2 ⊂ Cage complex

Water insoluble iron catalyst **1-H_2O** has tetraphenylphosphonium as the counter cation instead of tetraethylammonium in **1**. Water insoluble catalyst was stirred overnight in a 1 ml solution of 2.5 mM cage so as to maintain 1:1 catalyst:cage ratio in D_2O for 6 days, Figure S5. The colorless cage solution changes to black overtime. The solution was filtered through a 0.45 μ filter. Characterization of the reaction mixture was done through NMR and UV visible absorption.

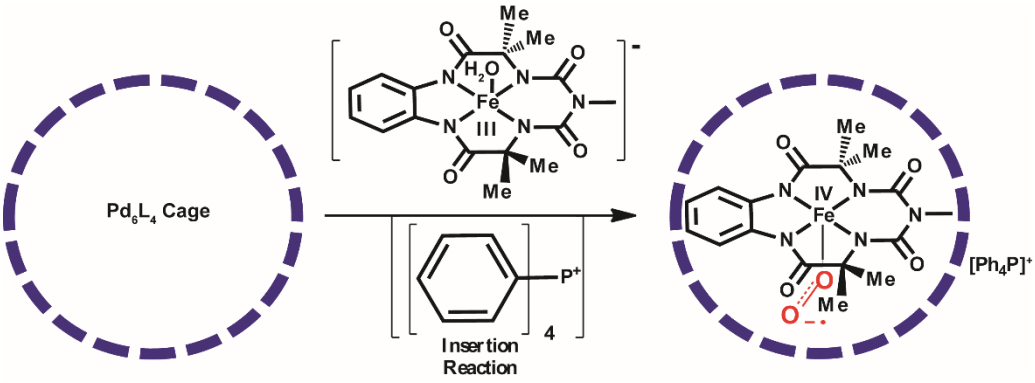

Figure S5. Representation of the insertion reaction of Fe (III)-biuret catalyst with a counter cation tetraphenyl phosphonium (1-H_2O[Ph_4P]) in a solution containing dissolved Pd-cage. Tetraphenyl phosphonium cation makes the catalyst water insoluble, and generates **1-O_2** ⊂ Cage in cage solution.

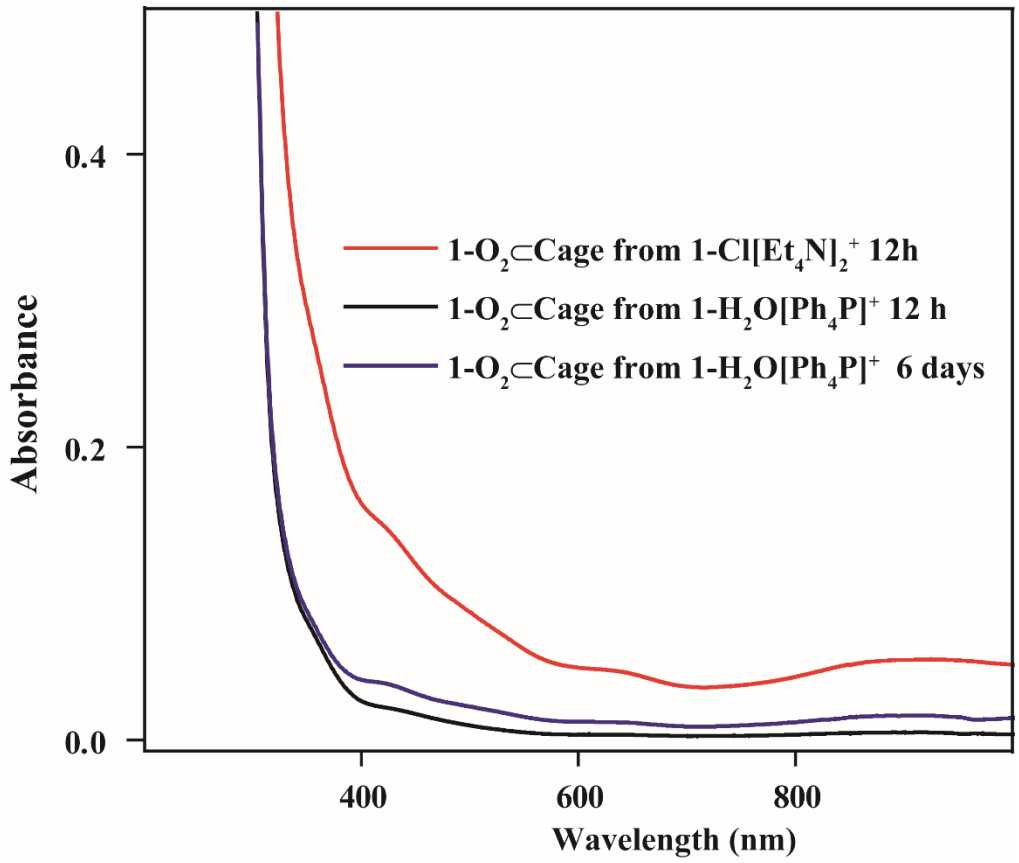

Figure S6. Solution state absorption spectra of **1-O_2**⊂Cage from 1-Cl[$\boldsymbol{Et_4N}$]$_2$ (~100 μM in H_2O, in red), **1-O_2**⊂Cage from 1-H_2O[Ph_4P] after 12 h (25 μM in H_2O, black), **1-O_2**⊂Cage from 1-H_2O[Ph_4P] after 6 days (25 μM in H_2O, blue).

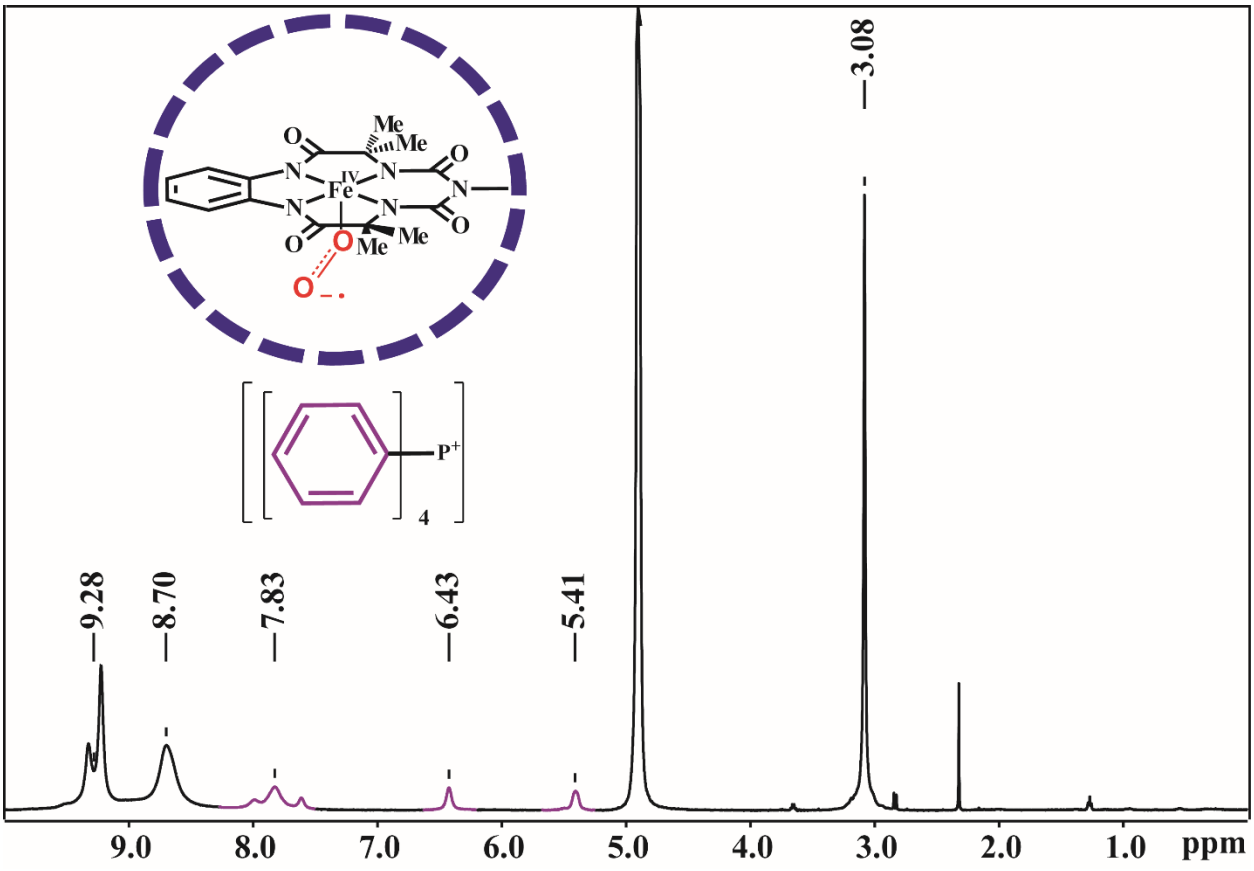

Figure S7. ^{1}H NMR of inclusion complex **1-O_2**⊂Cage from 1-H_2O[Ph_4P] (600 MHz, 298 K).

5. Displacement and anion exchange of 1-O_2 ⊂ Cage complex

2 mM of **1-O_2** ⊂ Cage solution was treated with 20 mM 9-Methylanthracene (MeAn) for 12 h. **Figure 4** present a schematic representation of the displacement reaction. Post reaction the solution was characterized by steady state UV-Visible absorption measurements.

Above reaction mixture was treated with excess Potassiumhexafluorophosphate (KPF_6). The nitrate counter anion for the palladium nanocage is replaced with hexafluorophosphate anion (PF_6^-) and the cage complex along with its guest precipitate out of the solution. The turbid solution is centrifuged, catalyst being water soluble stays in the solution the precipitate is separated from supernatant and taken for absorption spectrum. Anion exchange can be better visualized with help of Figure 5.

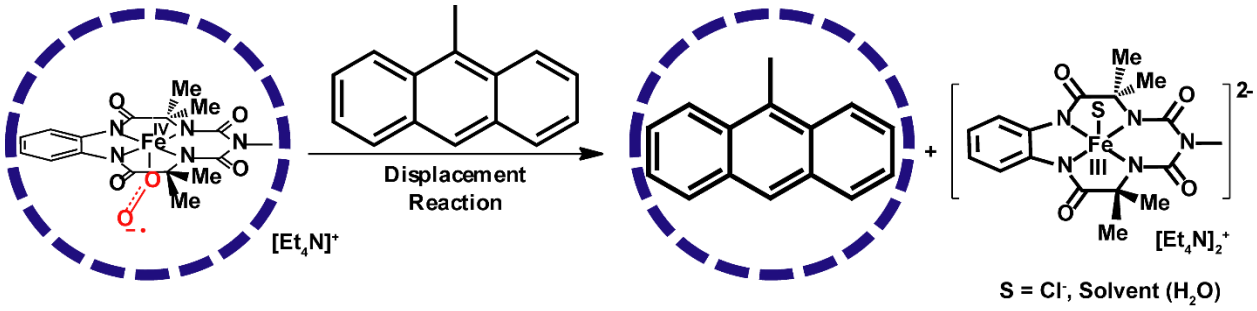

Figure S8: Representation of displacement reaction. MeAn is water insoluble and it displaces water soluble catalyst out once it moves inside the cavity.

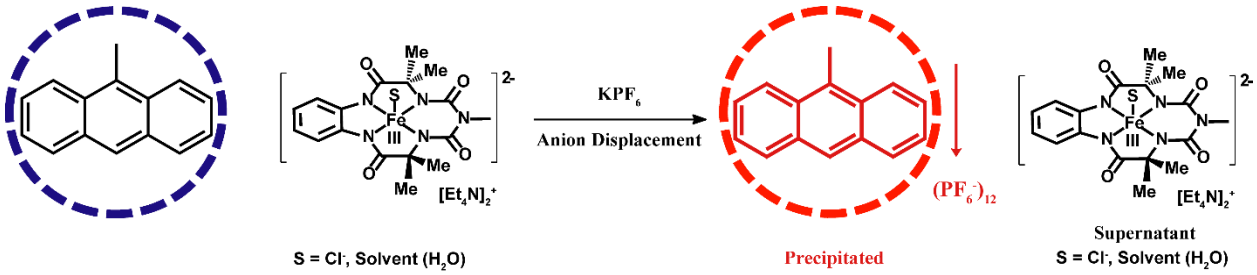

Figure S9: Anion exchange reaction represents, PF_6^- replaces the NO_3^- anion of the nanocage leading to precipitation along with guest. Catalyst being water soluble stays in the solution and can be separated by centrifugation.

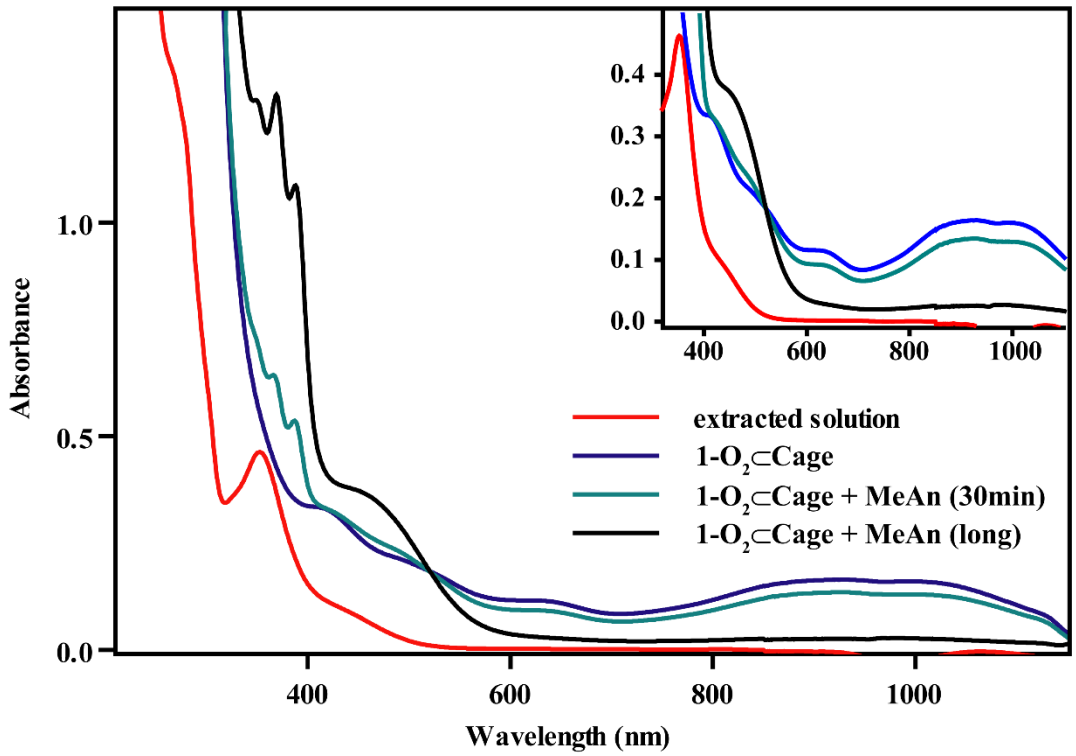

Figure S10. Steady state absorption spectra of **1-O₂** ⊂ Cage (in blue), **1-O₂** ⊂ Cage treated with MeAn for 30 min (green), **1-O₂** ⊂ Cage treated with MeAn for 12 h (black), absorption spectrum of supernatant collected after treatment KPF_6 (red). Inset: zoomed from 350 nm to 1100nm.

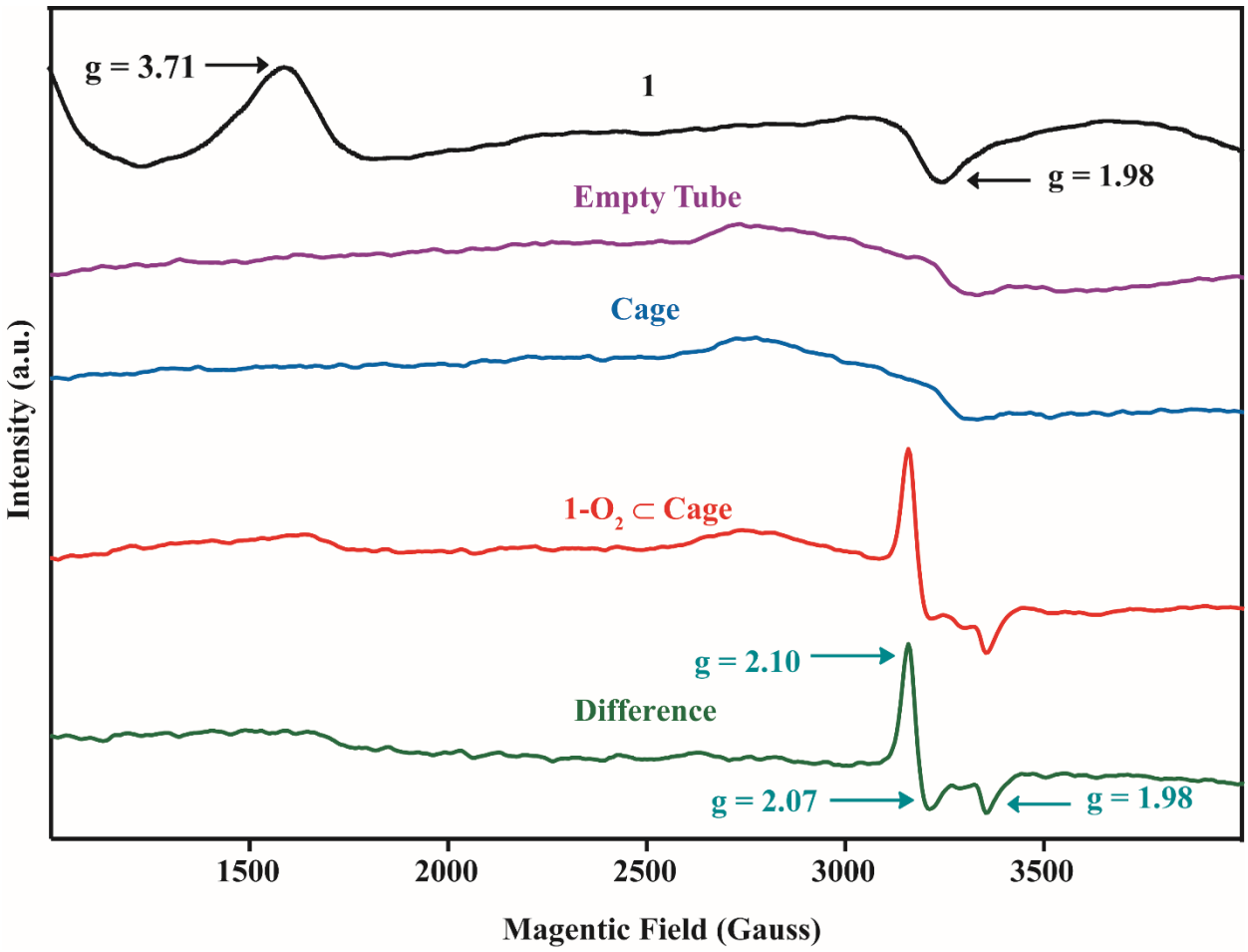

Figure S11. Comparative EPR spectra of the free catalyst 1-Cl[$\boldsymbol{Et_4N}$]$_2$ (black) in water, empty EPR tube, Cage (blue), **1-O$_2$** ⊂ Cage (2 mM in H_2O, red), and difference spectrum (**1-O$_2$** ⊂ Cage – Cage). All spectra were recorded at 93 K with modulation amplitude of 1 G and at 0.2 mW MW power on a X–band Bruker EMX EPR spectrometer. The background in the cavity is illustrated by the empty EPR tube spectrum.

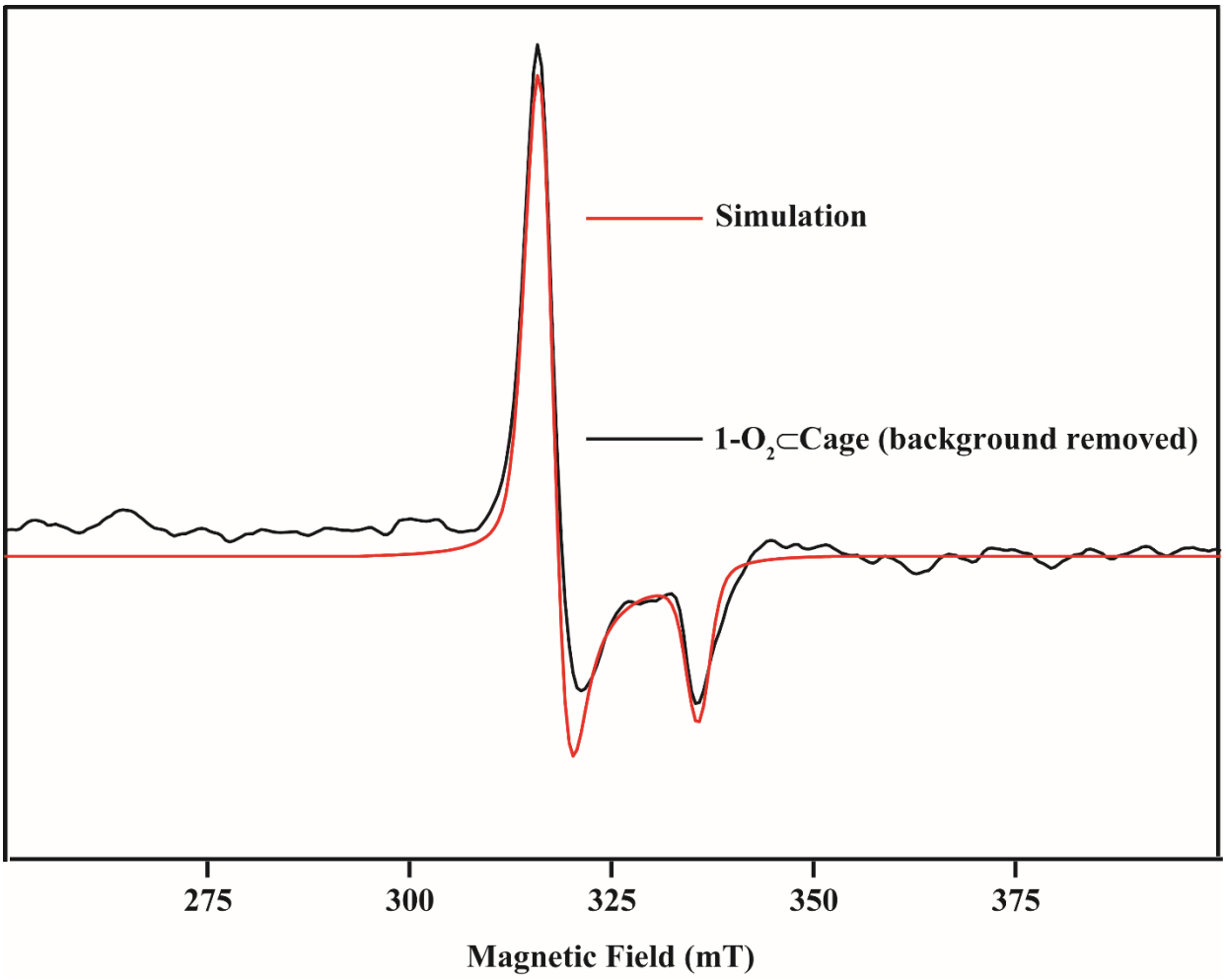

Figure S12. EPR spectrum of **1-O$_2$** ⊂ Cage and its simulation is plotted. The g values obtained from simulation is $g_{xx} = g_{yy} = 2.102$, $g_{zz} = 1.985$ corresponds to S = ½ species. The simulation is vertically offset from the raw data for clarity.

6. Chemical synthesis of Fe^{IV}-superoxo complex

To a solution of **[**$Et_4N]_2[(bTAML)Fe^{III}(Cl)]$ (1-Cl[$\boldsymbol{Et_4N}]_2$) (20 mg) in DCM, was added excess (~10 equivalent) of ceric ammonium nitrate (CAN) and the solution was stirred for 5 min. The resulting violet color solution was filtered, and UV-Vis spectrum was recorded. Absorbance at wavelength 543 (ε = ~ 5000 cm^{-1} M^{-1}) nm and 857 nm (broad) (shown in **FigureS13**) confirm the formation of $[Fe^{IV}(Cl)$-bTAML$]^-$. (Singh, K. K.; Sen Gupta, S. *Chem. Commun*. **2017**, *53*, 5914-5917). Further, complex $[(bTAML)Fe^{IV}(Cl)]^-$ (X-band EPR silent) upon reaction with potassium superoxide (KO_2) in DCM at -40 °C, showed a *S*=1/2 spin EPR signal ($g_x = g_y = 2.12$ and $g_z = 1.996$) (**Figure S14**).

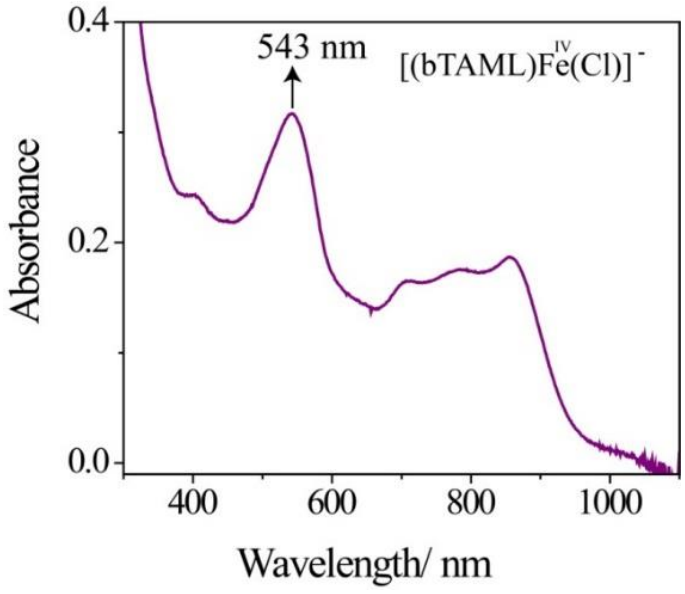

Figure S13. UV-Vis spectrum of complex $[(bTAML)Fe^{IV}(Cl)]^-$ in dichloromethane.

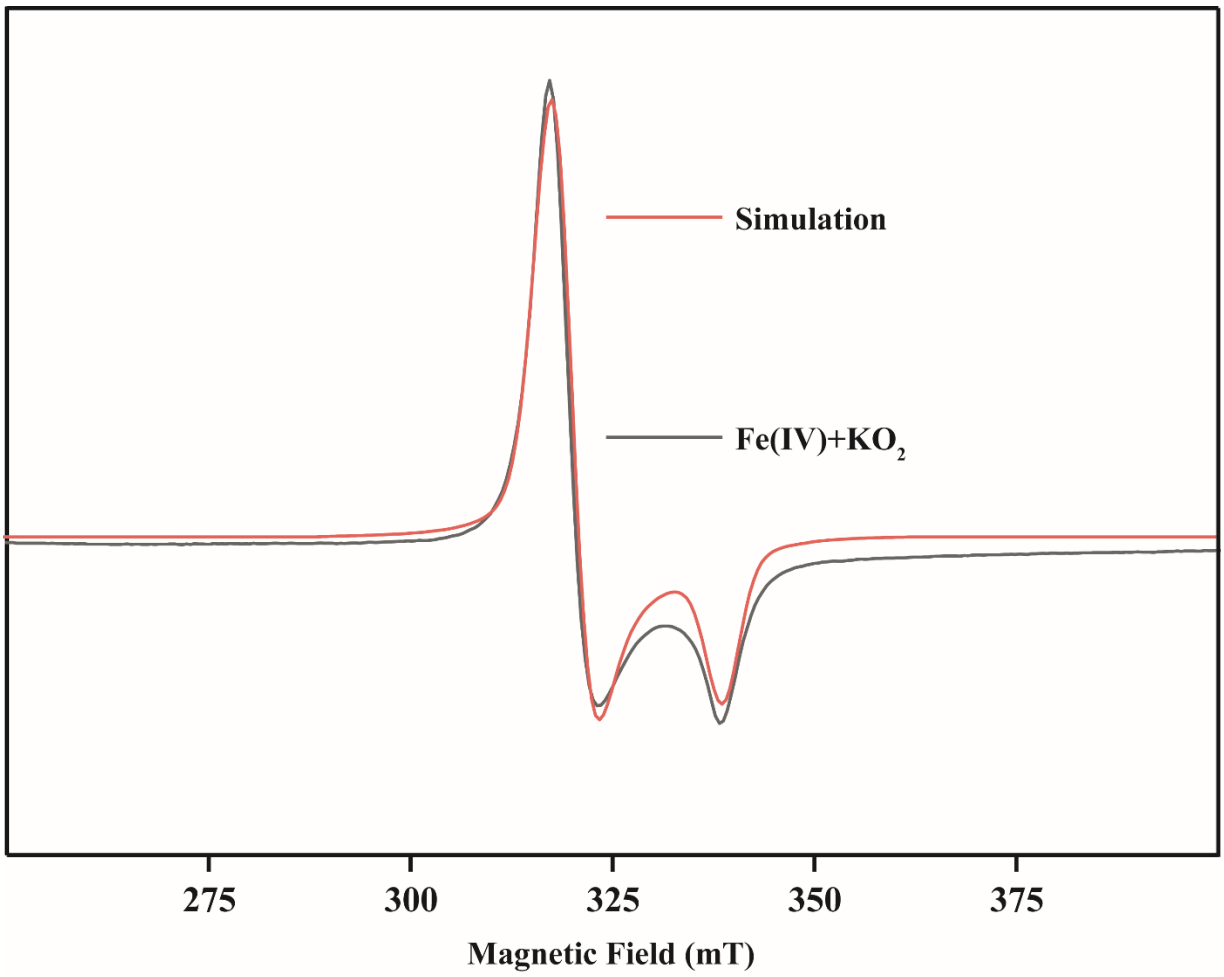

Figure S14: The X-band EPR of resulting solution after reaction between Fe^{IV}-Cl and KO_2; and the corresponding simulation. The axial g-tensor has principal values of $g_x = g_y = 2.12$ and $g_z = 1.996$ representing Fe(IV)-superoxo species.

7. Resonance Raman spectroscopy of the inclusion complex 1-O_2 ⊂ Cage in isotopically labeled water ($H_2{}^{18}O$ and $H_2{}^{16}O$):

1-O_2⊂Cage was prepared in two different isotopically labeled water solutions of $H_2{}^{18}O$ and $H_2{}^{16}O$ from 1-Cl[$\boldsymbol{Et_4N}$]$_2$. Due to small volume the Raman spectrum of $H_2{}^{18}O$ sample was measured in static condition while sample in $H_2{}^{16}O$ was measured in flowing condition. These measurements were performed using a 532 nm laser as the excitation source and acquisition was averaged over 10 scans with total acquisition time of 120s. The power at the sample was measured to be 2.5 mW for both samples. Apart from the shift in low frequency shift in the samples prepared in differently labeled water, different features in the spectrum were also found to be sensitive. The feature though poor to signal to noise make it harder to confirm the shift observed thus different normalization ratio has to be implemented to observe dispersive feature in different regions of the spectrum as shown in the Figure S15. Based on previous work of Nakamoto and coworkers, and other groups the features sensitive to isotopic labeling were assigned. The feature at 1086 cm^{-1} is assigned to νO-O which in $H_2{}^{18}O$ sample is partly hidden in 1063 cm^{-1} feature of the cage. The feature at 697 cm^{-1} is part of oxygen isotope sensitive bands in the region of 600-800 cm^{-1} is assigned to the side on isomer ν(Fe-O) stretching mode coupled to vibrations of ligand around Fe center.

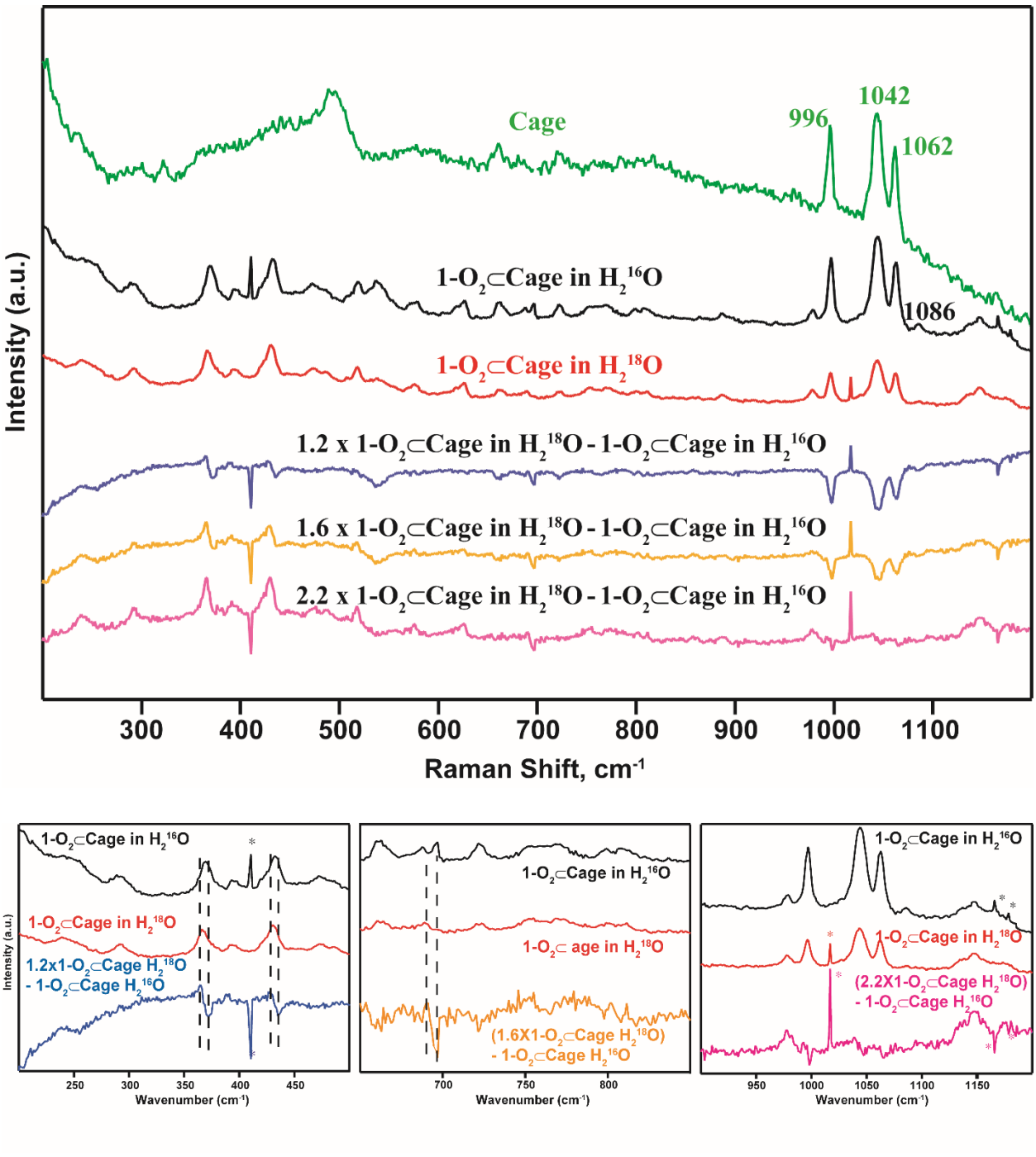

Figure S15. Top: Resonance Raman of Cage (in green), **1-O$_2$⊂**Cage prepared in $H_2{}^{16}O$ (in black), **1-O$_2$⊂**Cage prepared in $H_2{}^{18}O$ (in red) and different ratio of normalizations to see isotopically sensitive features; **Bottom:** Resonance Raman spectrum of **1-O$_2$⊂**Cage prepared in $H_2{}^{16}O$ (in black), **1-O$_2$⊂**Cage prepared in $H_2{}^{18}O$ (in red) and difference spectrum spectra ($H_2{}^{18}O$ spectrum – $H_2{}^{16}O$ spectrum, in blue) in different regions, * depict cosmic rays

ST1: Vibrational peak representative of ($Fe(IV) - O_2^-$) formation in 1-$O_2 \subset$ Cage

	in $H_2{}^{16}O$	in $H_2{}^{18}O$	$\Delta = H_2{}^{18}O - H_2{}^{16}O$
ν(Fe-O-O) end-on isomer	372 cm^{-1}	365 cm^{-1}	7 cm^{-1}
ν_a(Fe-O_2) side-on isomer	435 cm^{-1}	427 cm^{-1}	8cm^{-1}

8. Synthesis of the inclusion complex 1-O_2⊂Cage in different isotopes molecular oxygen environment:

A three neck flask was attached with a Schlenk line that is connected to argon and vacuum, a balloon to perform maintain reaction under a particular gaseous environment, and septa to inject sample. The set up was purged with argon and vacuumed thrice and kept under argon atmosphere. 1 ml of 2mM cage solution was injected through the septa. The three neck flask was put into liquid nitrogen bath to freeze the solution and the gas from the top of the solution was evacuated with the help of vacuum. Vacuum was stopped and argon was reintroduced in the reaction vessel and the vessel was brought to room temperature. This process of freeze, vacuum, argon purging and thaw was performed 3 times to remove dissolved oxygen in the solution. Under constant flow of argon 1.4 mg of catalyst 1-Cl[$\boldsymbol{Et_4N}$]$_2$ was added to the reaction vessel and then sealed off still under argon atmosphere. The freeze, vacuum, argon purging and thaw cycle was performed again 2 times. The third time after vacuum step the vessel was purged with $^{18}O_2$ and the atmosphere was maintained for the reaction vessel because of the balloon attached. The insertion reaction was carried out for 12 h similar to the reaction under ambient conditions. After the reaction is over the sealed vessel was moved into a glove bag that has been purged with argon and vacuum thrice. The reaction vessel was opened and filtered, put in cuvette for Raman measurements attached to a sealed stock container. The measured Raman spectrum for sample prepared in $^{18}O_2$ and $^{16}O_2$ (ambient conditions) and their difference, is shown in **Figure S16**.

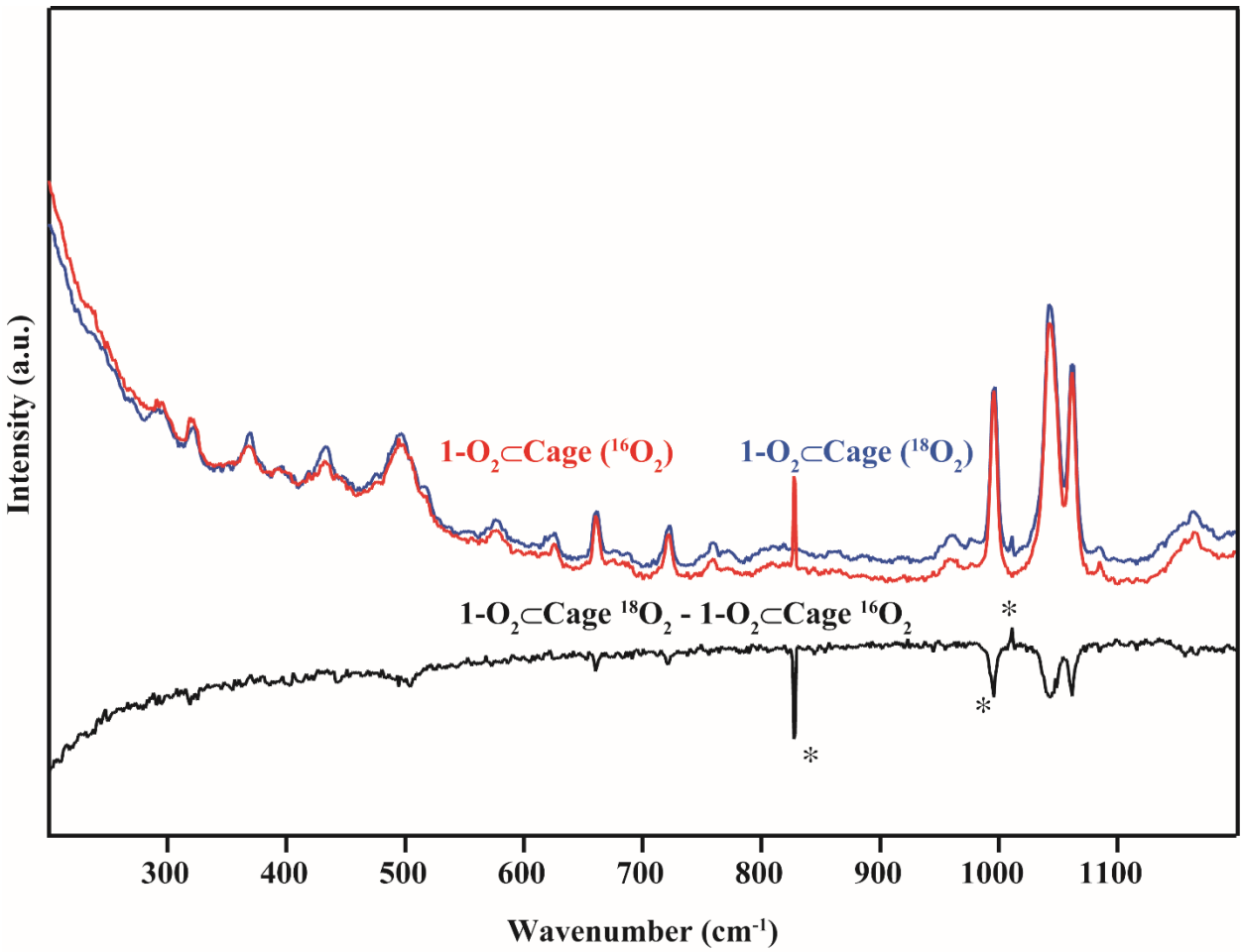

Figure S16. Resonance Raman of **1-O_2** ⊂ Cage prepared in $^{16}O_2$ (in red), **1-O_2** ⊂ Cage prepared in $^{18}O_2$ (in blue), difference spectra (0.8*$^{18}O_2$ spectrum – $^{16}O_2$ spectrum, in black) (* depict cosmic rays). We observe no changes in the modes associated with 18O-isotope enrichment. The label was washed away by 55 M $H_2{}^{16}O$ as expected.